Geomechanics and Engineering, *Vol. 24, No. 1 (2021) 1-14*
DOI: https://doi.org/10.12989/gae.2021.24.1.001

Evaluation of grout penetration in single rock fracture using electrical resistivity

Hangbok Lee[1a], Tae-Min Oh*[2] and Jong-Won Lee[2b]

[1]*Center for Deep Subsurface Research, Korea Institute of Geoscience and Mineral Resources (KIGAM), 124 Gwahak-ro, Yuseong-gu, Daejeon 34132, Republic of Korea*
[2]*Department of Civil and Environmental Engineering, Pusan National University (PNU), 2 Busandaehak-ro 63beon-gil, Geumjeong-gu, Busan 46241, Republic of Korea*

(Received January 16, 2020, Revised November 3, 2020, Accepted November 7, 2020)

Abstract. In this study, a new approach using electrical resistivity measurement was proposed to detect grout penetration and to evaluate the grouting performance for such as waterproof efficiency in single rock fracture. For this purpose, an electrical resistivity monitoring system was designed to collect multi-channel data in real time. This was applied to a system for grout injection/penetration using a transparent fracture replica with various aperture sizes and water-cement mix ratio. The electrical resistivity was measured under various grout penetration conditions in real time, which results were directly compared to the visual observation images of grout penetration/distribution. Moreover, the grouting success status after the curing process was evaluated by measuring the electrical resistivity in relation to changes in frequency in fracture cells where grout injection and penetration were completed. Consequently, it was determined that the electrical resistivity monitoring system could be applied effectively to the detection of successful penetration of grouting into a target area and to actual field evaluation of the grouting performance and long-term stability of underground rock structures.

Keywords: electrical resistivity; grout penetration; grouting performance; waterproof efficiency; aperture sizes; water-cement mix ratio

1. Introduction

Recently, the utilization of underground space has intensified for the construction of subsea tunnels, disposal of radioactive waste, and energy storage (e.g., hydrocarbon oil and gas) at great depth (Broch 2007, Gueddouda *et al.* 2010, Wang *et al.* 2015). To construct and operate such deep underground facilities, grouting techniques provide an important method of reinforcement to prevent water leakage and to enhance rock strength for better mechanical stability (Kobayashi *et al.* 2014, Zhang *et al.* 2014). Without the proper application of grouting to underground facilities, structural safety and operational conditions cannot be guaranteed (Axelsson *et al.* 2009, Lisa *et al.* 2012, Rafi and Stille 2014, Zhang *et al.* 2017).

The grout materials are mixed with water to allow the rock grouting to flow better. This mixture is then injected into drilled boreholes. From there, the grout penetrates any voids or fractures that cross-connect with the field boreholes. In the end, the aim is for the grout material to fill any voids and fracture networks within the rock mass near the underground facility. In this case, when heterogeneous fractures are distributed around the underground space, there may remain unexpected areas where the injected grout has not penetrated. In some cases, this could require the input of additional grout into areas outside the originally designed grouting zone (Kim *et al.* 2018). Therefore, understanding grout penetration and distribution behaviors is very important for efficient rock grouting performance for a successful waterproof structure (Funehag and Fransson 2006, Saeidi *et al.* 2013, Mohajerani *et al.* 2015, Mohammed *et al.* 2015). In addition, it is necessary to optimize the design of grout injection plans to include the accurate detection or monitoring of grout penetration (Lunn *et al.* 2018).

Several methods have been proposed for evaluating grout penetration and distribution. Majer *et al.* (1989) proposed a seismic monitoring method based on high-frequencies for detecting grout penetration in real time. However, they did not correlate seismic activity data to the location of the injected grout. Chen *et al.* (2000) observed the grout distribution pattern using a fluorescent approach, but this was an intrusive method requiring bulky equipment such as a downhole television logging system. Moreover, it was also not suitable for real-time monitoring. Henderson *et al.* (2008) used a pH monitoring method for tracking the real-time spread of ultrafine grout in a shaft at Dounreay containing nuclear waste. However, there was a mismatch between the pH values and the penetration front of the grout.

Non-destructive geophysics techniques such as ground penetrating radar (GPR) were applied to the detection of the grout distribution behind the lining segments of shield tunnels (Zhang *et al.* 2010). However, the grout was only detected at distances less than one meter and there was too

*Corresponding author, Assistant Professor
E-mail: geotaemin@pusan.ac.kr
[a]Ph.D.
E-mail: leehb@kigam.re.kr
[b]Ph.D. Candiate
E-mail: lee.j@pusan.ac.kr

ISSN: 2005-307X (Print), 2092-6219 (Online)

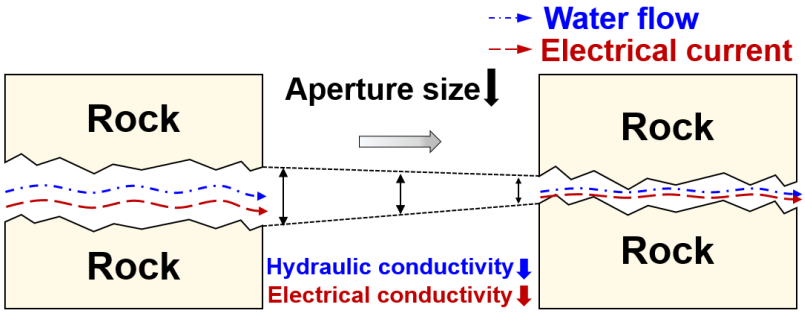

Fig. 1 Basic mechanism of electrical resistivity monitoring

much noise in the data due to utility infrastructure (e.g., power cables) within the tunnel. This technique also has other drawbacks: real-time detection is difficult due to the slow speed of GPR data collection. Moreover, whole cross-section scanning is needed, which involves great cost and effort. Thus, a new direct and cost-effective method to overcome the shortcomings of existing methods is needed for accurate, real-time detection of injected grout.

In this study, a new method using the measurement of electrical resistivity (ER) was proposed to detect grout penetration and to evaluate grouting performance in rock fractures. Moreover, the feasibility of this non-destructive method was verified by comparing measured electrical resistivity and visual observations of grout penetration/distribution in laboratory experiments. For this, we designed a compact ER monitoring system and a system for monitoring grout injection and penetration using a transparent fracture replica with various aperture sizes and water-cement (w/c) mix ratios. In addition, the correlation between the normalized ER values and grouting status within rock fractures after completing the curing process was evaluated by monitoring the ER in relation to change of signal frequency. This result is closely related to the rock grouting performance indicated by waterproofing efficiency. Finally, we discuss the field applicability of our ER system for the detection of grout penetration and distribution, as well as for long-term monitoring of grouting performance and stability in underground rock structures.

2. Background concept

For underground space within fractured rock, no researcher has studied direct detection of grout penetration and distribution using the ER method. Compared to other kinds of geophysical survey, the ER monitoring system has considerable advantages: Changes of electrical resistivity are instantaneous and apparent according to the movement of an electrically charged fluid such as the hydrated grout materials. Moreover, an electrode sensor installed in a grouting borehole can monitor the degree of grout filling, which indicates the long-term waterproofing performance. This approach is also economical because it requires only small, simple equipment with low-cost electrode sensors.

The basic mechanism of electrical resistivity monitoring used in this study is as follows. When an ionic fluid migrates through open channels, an electrical current is generated according to the fluid flow, as shown in Fig. 1. The hydraulic conductivity of groundwater is its ability to flow through porous media or rock fractures. Similarly, the electrical conductivity of a specific material is its capability to transfer ions in an electrical field. Generally, the electrical conductivity cannot be measured directly; hence, it is simply estimated by measuring the electrical resistivity, because the electrical resistivity value is inversely proportional to the electrical conductivity. The electrical resistivity is the ratio of the applied potential difference and the electrical current generated. This value varies greatly with the properties (e.g., electrical conductivity, geometry of the rock fracture) of the surrounding materials and the temperature, assuming that the rock does not conduct electrical current.

Grout includes a group of cement-based materials that present a wide range of electrical resistivity values (Madhavi and Annamalai 2016). Similar to clay paste, wet grout material is a substance with a strong electrical charge, and it behaves as a strong conductor that can transfer large amounts of ions before hardening. However, once the grout has cured over time, it acts as an insulator much as hard rock stone does. Thus, a grout material might exhibit low electrical resistivity when wet and have much higher resistance when dry. Because natural groundwater contains small amounts of mineral ions, its electrical resistivity is high, except for special cases such as salt-water (brine) or water in clay layers (Keller and Frischknecht 1996). Therefore, the injection of grout containing many ions should decrease the bulk electrical resistivity. This apparent change could serve as an indicator for detecting the penetration and distribution of grout injected into underground facilities in fractured rock aquifers.

3. Materials and methods

3.1 Experimental materials

A In this experiment, micro cement (MICEM 8000, SsangYong Cement, South Korea) was used as the grout material. Micro cements are mainly used to enhance the strength of weathered rock and to prevent water leakage into underground rock spaces (Eriksson 2002, Northcroft 2006, Panthi and Nilsen 2010, Stille *et al.* 2012, Khave 2014). In deep underground rock spaces, individual rock joints called fractures have very small apertures (less than a

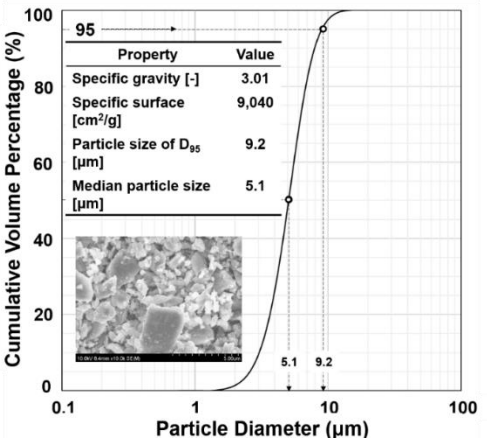

Fig. 2 Properties and grain size distribution curve of MICEM 8000 micro cement

Fig. 3 Micro cement for grouting injection: Powder (left), Fluid mixture (right)

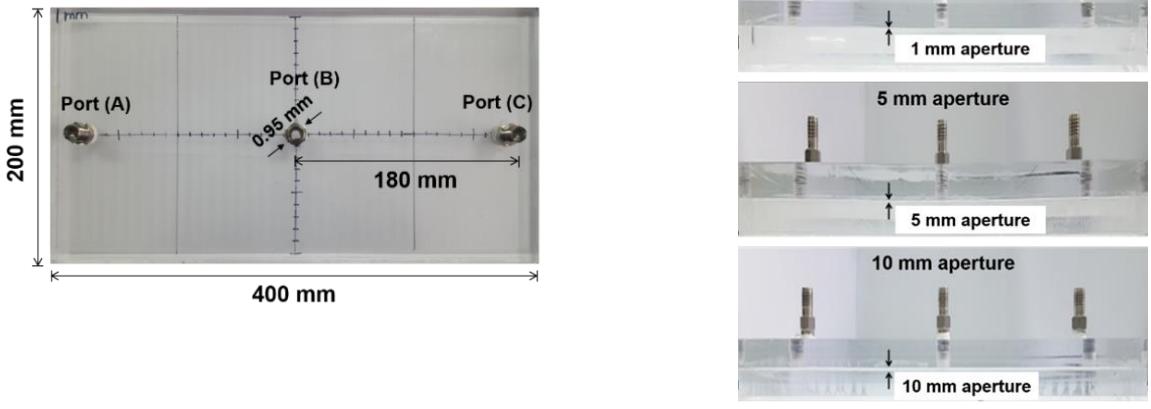

(a)

Fig. 4 Artificial fracture cells including inlet/outlet ports with different apertures: (a) Top view and (b) Side view of fracture

millimeter) due to high in situ vertical stress. Hence, it is difficult for ordinary cement such as Portland cement to penetrate and be distributed into fine rock fractures. Fig. 2 shows the physical properties and grain size distribution of the micro cement.

Fig. 3 shows pictures of the original micro cement powder and of the wet mixture (fluid). For rock grouting, the grout fluid is a mixture of water and cement powder. During injection, the water-cement mix ratio (w/c) becomes a crucial factor for evaluating the penetration and distribution of the grout injected into boreholes. This is because the w/c ratio is directly related to the fluidity and bleeding of the grout mixture. Previous research used grout with a w/c range from 0.5 to 1.0 (Høien and Nilsen 2014). In this study, the w/c ratios were divided into low (0.6) and high (1.0) categories. The viscosity values at low (0.6) and high (1.0) w/c ratios were 327 and 22 centipoise (cP), respectively (the viscosity of water is 1 cP) (Lee *et al.* 2017). Low and high w/c values were 15 times different in viscosity value. This means that the grout can penetrate well

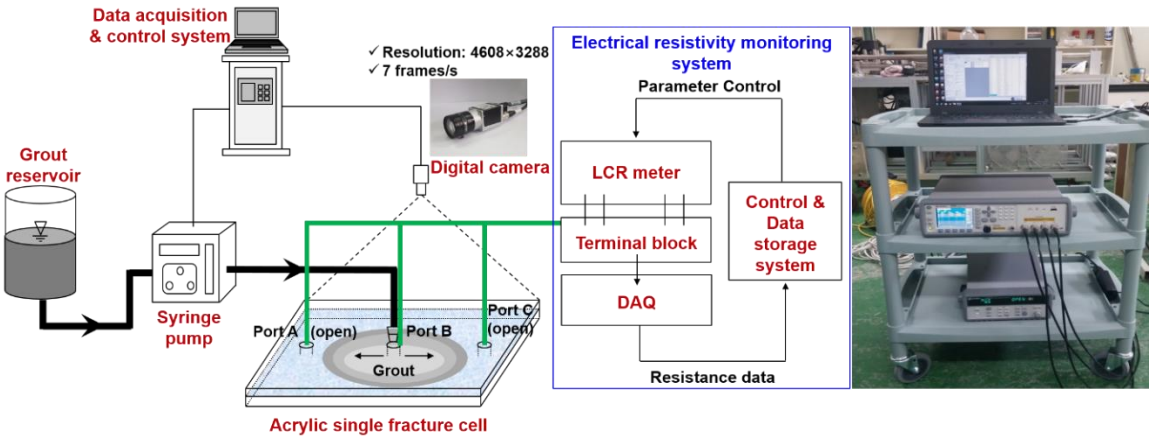

Fig. 5 Schematic of the electrical resistivity monitoring setup used for detecting the penetration behavior of grout

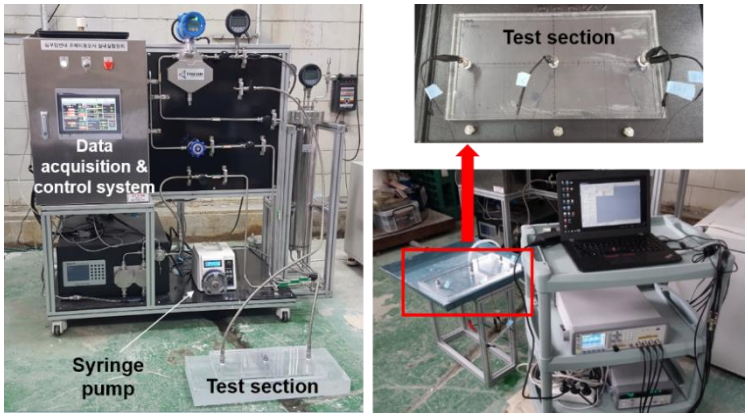

Fig. 6 Grout injection system

into rock fractures under the high w/c condition. Note that, other chemical additives for grout hardening and improvement were not considered in this experiment.

Fig. 4 shows an artificial fracture cell for evaluating penetration and distribution behaviors of grout using the ER monitoring system. The cell was designed as a rectangular acrylic parallel plane model with a fracture size of 200 mm (width) × 400 mm (length) with different aperture sizes (1, 5, and 10 mm). Direct visual observations of the penetration of grout fluids were possible in real time using this transparent fracture replica.

The International Society for Rock Mechanics (ISRM 1978) proposed that rock joints with apertures between 0.5 and 10 mm would be pathways for flowing fluids in grouting implementation. Therefore, fracture cells with aperture sizes of 1-10 mm were made and used in this experiment. Three ports were added: a grout injection point (B) and two drainage points (A and C). The inner diameter of all ports, and the distance between ports was 0.95 mm and 180 mm, respectively. These ports were made of stainless steel, and they also served as the electrode sensors in the electrical resistivity system. The boundary of a cell was completely sealed, and thus injected grout or water only migrated through interior fractures of the system.

3.2 Experimental setup

The total set of laboratory experiments was divided into two major parts: the electrical resistivity monitoring system and the grout injection system. First, Fig. 5 shows the actual image and conceptual diagram of the electrical resistivity system. It was composed of three parts: (1) LCR meter devices capable of measuring electrical resistance, (2) a data acquisition (DAQ) device capable of continuously collecting multi-channel data, and (3) a controller for controlling the input electrical voltage, current, and frequency; and for storing the measured data received from multiple channels over a long interval.

This system was established for detecting the grout penetration and distribution, and was adjustable from 0 Hz (DC) to a maximum of 2 MHz. The input voltage range was adjustable from a minimum of 0.1 V to a maximum of 20 V. Moreover, 20 channels were configured to enable ER monitoring at multiple measurement points.

Fig. 6 shows the grout injection system for conducting penetration tests. It was composed of three parts: (1) syringe pump, (2) control and data acquisition systems, and (3) test specimen section. In this experiment, the syringe pump was used to inject grout into the artificial fracture. This pump had the ability to inject precise amounts, from a minimum of 100 mL to a maximum of 6000 mL per minute. The control and data acquisition systems were installed to control the experimental parameters and to acquire data. A digital camera was used to observe and record visual images of the penetration and distribution of the grout after

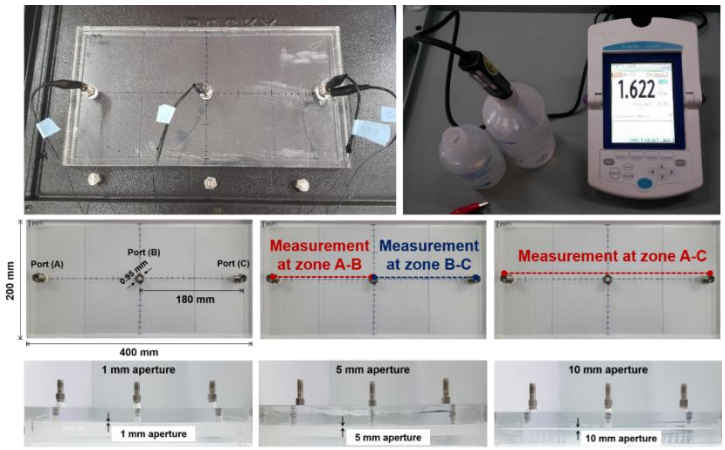

Fig. 7 Calibration of electrical resistivity system using shape factor

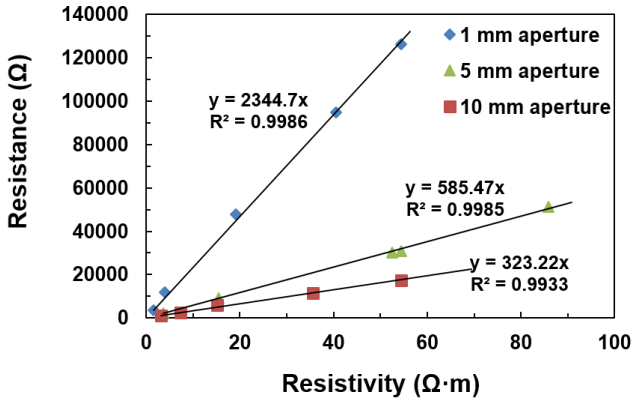

Fig. 8 Correlation between electrical resistance and resistivity relative to aperture size at 1 V and 10 kHz

injection. This visual device had a display resolution of 4608 × 3288 (15 million pixels) and could record moving images at seven frames per second.

3.3.1 Grout injection

For injection of the grout material into the test cell, micro cement was mixed with water under constant conditions (w/c = 0.6/1.0). Mixtures were sufficiently stirred within one minute at room temperature (23 ± 1°C). Mixing was performed using the EUROSTAR 200 digital overhead stirrer. The stirring quantity was 100 L, the torque was 200 Ncm, and rate was 30 to 2000 rpm (revolutions per minute). The stirring time was one minute and rotation speed was 1200 rpm. After mixing, the grout in the reservoir tank was immediately injected into the single fracture cell through a syringe-dedicated hose.

To reproduce an actual rock fracture saturated with groundwater in a deep underground environment, the fracture cell was fully pre-saturated with water before starting the grout injection. The predetermined grout injection rate was 200 mL/min, because this was the minimum rate that avoids stagnation or clogging of the injected grout fluid within the syringe-dedicated hose. Grout fluids were injected into the center port (B) using the syringe pump. The open ports (A and C) acted as outlets during the grouting injection and penetration processes. Moreover, to confirm the condition of complete saturation of grout inside the fracture cell, grout was constantly injected until it overflowed from the two open ports. The complete grout behavior during injection and penetration was visually observed and recorded using a high-resolution digital camera.

3.3.2 Determination of input voltage and frequency

The electrical resistivity monitoring system was applied to the grout injection system for detecting the penetration and distribution of grout fluid injected into acrylic fractures. Three metallic ports acted as electrode sensors and were connected to the monitoring system. Electrical resistance values were measured using an LCR meter by applying an AC voltage to the test cell and by sensing the current flowing at that time. In this experiment, the resistance was measured under the conditions of 1 V and frequency of 10 kHz. To determine the frequency to be applied (i.e., 10 kHz), the change in resistance was explored in relation to frequency (from 20 Hz to 1MHz): the resistance was shown to be constant within the range 20–100 kHz.

3.3.3 Cell calibration for resistivity

Calibration tests to establish the relationship between electrical resistance and resistivity for the tested cells were initially performed in relation to NaCl solutions with distilled water. Electrical resistance was expressed as electrical resistivity through the calibration process for the

specific cells tested. The shape factor of test cells with dimensions of 200 mm (width) × 400 mm (length), different apertures (1, 5, and 10 mm), and electrodes of 5 mm diameter was determined by the following electrical resistance-resistivity correlation Eq. (1).

$$\rho \text{ (resistivity)} = \alpha \text{ (shape factor)} \cdot R \text{ (resistance)} \quad (1)$$

In the case of filling the test cell with NaCl solution, both electrical resistivity (by a conductivity meter) and resistance (by an LCR meter) were simultaneously measured to obtain the shape factor for calibration (Fig. 7).

Because electrical resistivity and resistance increase linearly, the relationship was measured by gradually adding increasing amounts of NaCl to the distilled water. Fig. 8 shows the correlation between electrical resistance and resistivity according to the aperture size obtained from the calibration experiments. Under the measurement conditions of 10 kHz and 1 V with series-mode measurement, the shape factor (α) of the fracture test cells were determined to be 0.0004, 0.0017, and 0.0031 m for aperture sizes of 1, 5, and 10 mm, respectively.

4. Results and analysis

The parallel acrylic fractures were initially filled with water (tap water in these experiments). In the beginning, the grout fluid injected (according to the aperture size and w/c) into the center port penetrated radially (formed a circular shape). After the grout reached the fracture side boundary, it gradually filled the interior of the fracture cell and continued to spread out toward the two outlet ports. With time, the grout fluid filled the entire test cell and overflowed through both outer ports. This time was considered the end of grout penetration.

4.1 Grout injection monitoring with w/c = 1.0

Fig. 9 shows visual images of the grout penetration behavior and the change of electrical resistivity with elapsed time for the case of aperture size 10 mm with w/c = 1.0. When the electrical resistivity was measured by transferring electrodes to both end ports (A and C), the initial value of the ER was 92 Ω·m before grout injection. According to previous research (Keller and Frischknecht 1996), the average resistivity value of natural fresh groundwater in areas of igneous rock is 90 Ω·m, which is very similar to that of tap water used in our experiments. Therefore, it can be judged that, in this experiment, tap water was reasonable substitute for the natural rock groundwater environment.

As the grout injection started, the electrical resistivity sharply decreased, as shown in Fig. 9. By the time that the grout injection was completed, the resistivity value decreased to 6 Ω·m and remained at that value thereafter. This reduction of resistivity is due to the high electrical property of the grout fluid. Clay-like material (e.g., micro cement) has high electrical charge compared to water (Oh *et al.* 2014). The injection of grout fluid containing many ions increased the electrical current flow and decreased the electrical resistivity. Therefore, as the grout penetrated the fracture test cell and its amount increased, the resistivity value fell lower and lower. The elapsed time (360 s) until the electrical resistivity decreased to its lowest value was identical to the time at which the grout injection and penetration was completed. Consequently, the change of electrical resistivity in real time reflected well the penetration and distribution behaviors of grout injected into the fracture cell.

For the case of aperture size 5 mm with w/c = 1.0, Fig. 10 shows visual images of the grout penetration behavior and the change of electrical resistivity with elapsed time. Similar to the previous experimental case (w/c = 1.0, aperture 10 mm), a radial penetration pattern was continuously observed until the grout injection was completed. However, with smaller fracture size (from 10 to 5 mm), the penetration rate of the grout fluid increased and the penetration was completed at a relatively earlier time (150 s). This result indicates that the grout penetration rate is inversely proportional to the aperture size, which corresponds with the results of the analytical solution suggested by Gustafson and Stille (1996).

The initial value of electrical resistivity measured in the fracture cell was 75 Ω·m before the grout injection. The final ER value was 3 Ω·m at the end of grout penetration, which is slightly lower than that of the previous experimental case (w/c = 1.0 and aperture size = 10 mm). The change of electrical resistivity was very clear according to the progress of grout penetration with elapsed time.

For the case of aperture size 1 mm with w/c = 1.0, Fig. 11 shows visual images of the grout penetration behavior and the change of electrical resistivity with elapsed time. At first, a large amount of air trapped in the syringe-dedicated hose was continuously injected instead of grout fluid. The region that appears brighter than the fracture cell represents the injected air. This air bubble could have formed due to the mixing or injection processes. After 30 s, properly injected grout spread out of the air-trapped area. A stratigraphic penetration pattern partially occurred due to the micro-fine furrows and ridges within the fracture formed during the manufacturing process. Although there were small differences in the grout penetration pattern at the early stage, a radial penetration pattern of a similar circular type after mid-term was commonly observed for all three cases (10, 5, and 1 mm apertures) at the same w/c ratio of 1.0. The penetration rate with aperture 1 mm was the fastest among the three cases, and the penetration process was completed after about 40 s from the start of grout injection.

Before the injection process, the initial electrical resistivity measured in the fracture cell was 70 Ω·m. When the air bubbles were first introduced into the test cell, the electrical resistivity suddenly increased to 255 Ω·m, as shown in the blue line of Fig. 11. This abrupt increase of electrical resistivity is because of the non-conductive property of air. As air with very high electrical resistance was injected, the resistivity value of the internal space between the electrodes of both side ports also increased due to this condition. Then, the electrical resistivity value dramatically decreased to 2 Ω·m after the grout fluid was properly injected into the fracture cell. The overall change of electrical resistivity well-matched the unusual injection and penetration process of air followed by the grout mix.

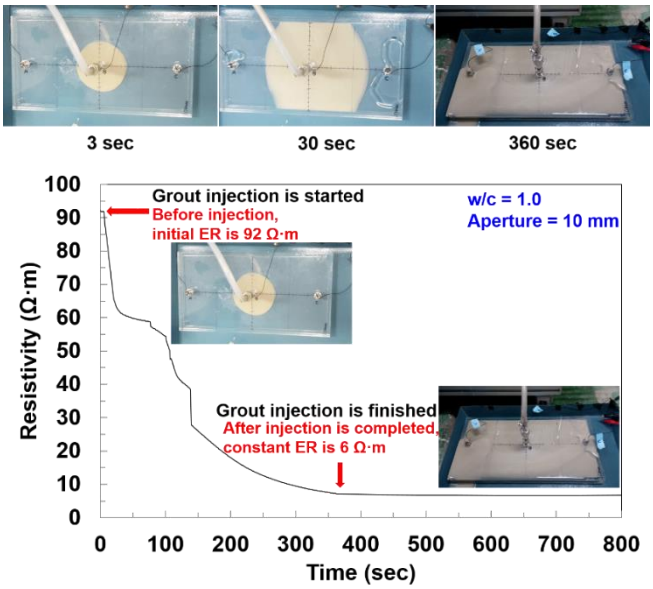

Fig. 9 Grout penetration images and electrical resistivity results with elapsed time for w/c = 1.0 and aperture size = 10 mm

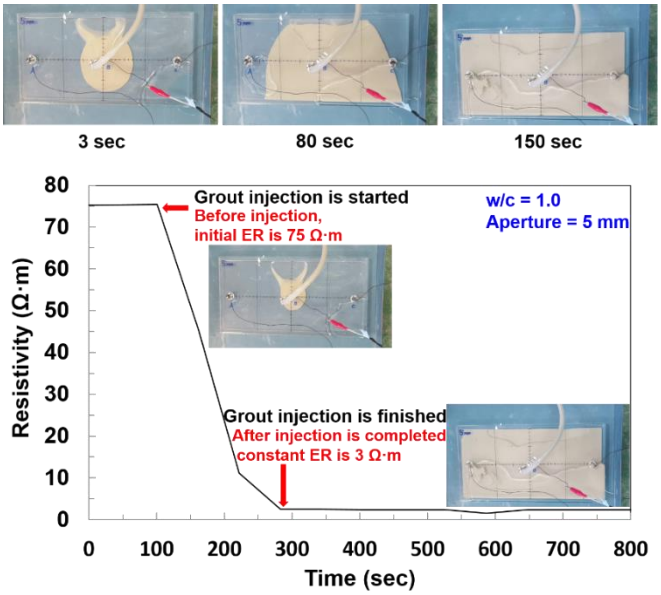

Fig. 10 Grout penetration images and electrical resistivity results with elapsed time for w/c = 1.0 and aperture size = 5 mm

As mentioned earlier, air injection could occur during the mixing and injection processes in actual in situ grouting operations. Especially in situations with grout injection at high pressure and great depth, more air bubbles could be generated by the formation of turbulent flow. These air bubbles trapped within the grout mixture could become potential pathways for water leakage if the grout ever corroded or deformed over the long term. This could greatly degrade the grouting performance for such as waterproofing efficiency. Therefore, the monitoring of unexpected air injection and distribution is important for ensuring grouting performance. If air was injected into a target space, the electrical resistivity would increase until proper grout injection was achieved. From this perspective, the electrical resistivity monitoring system can detect ordinary situations such as successful grout penetration, as well as abnormal situations such as air injection.

4.2 Grout injection monitoring with w/c = 0.6

Fig. 12 shows visual images of the grout penetration behavior and the change of electrical resistivity with elapsed time for the case of aperture size 10 mm and w/c = 0.6. Compared to the case of the same aperture size at w/c 1.0, similar grout penetration in a circular shape was also found, although a slight dilution boundary was observed in the area between the grout plume and the pre-saturated water in this case. The only major difference between the two cases was the penetration speed, which was due to the viscosity effects from a different w/c ratio. The time to fill the fracture cell fully with aperture size 10 mm was 360 and 440 s at w/c = 1.0 and 0.6, respectively. As the w/c ratio decreased, the grout fluid moved more slowly because of increased viscosity (22-327 cP). This experimental case also showed a good correlation between the electrical resistivity

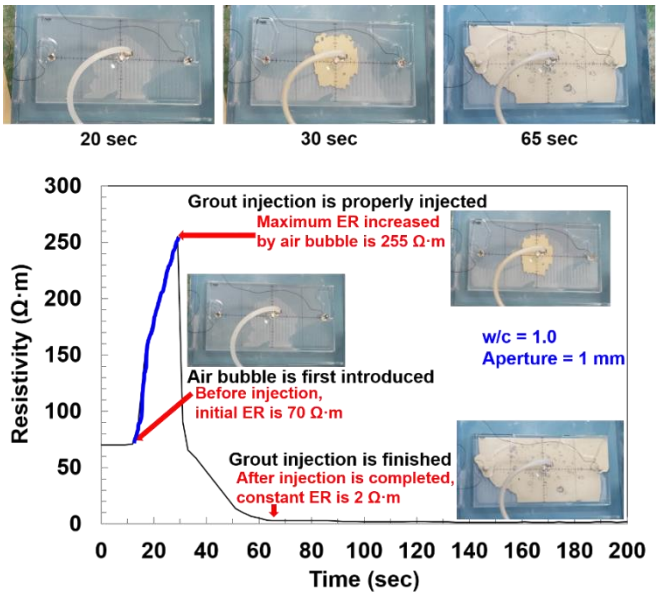

Fig. 11 Grout penetration images and electrical resistivity results with elapsed time for w/c = 1.0 and aperture size = 1 mm

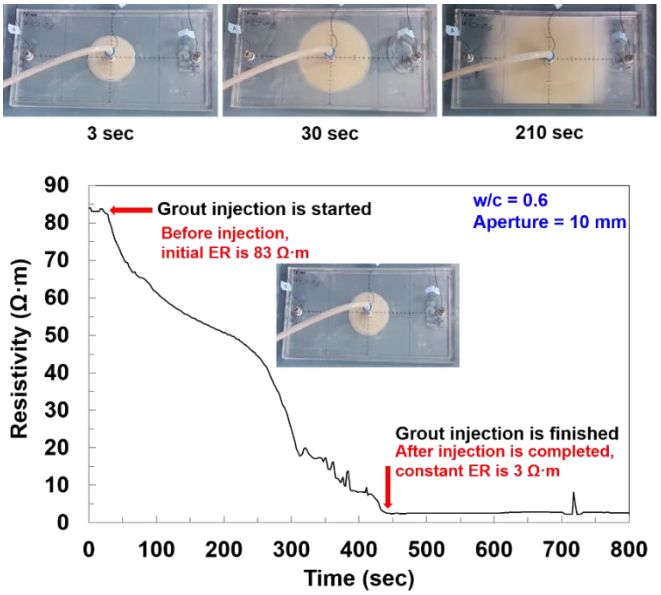

Fig. 12 Grout penetration images and electrical resistivity results with elapsed time for w/c = 0.6 and aperture size = 10 mm

value and visual image of grout penetration. During the 440 s from start to finish of the grout injection process, the ER showed a steep decline from 83 to 3 Ω·m.

There was a difference in the water-cement mix ratio values between the Fig. 9 (w/c = 1.0 and aperture size = 10 mm) and Fig. 12 (w/c = 0.6 and aperture size = 10 mm). As the mix ratio decreased, the cement-grout content increased, which means an increase of the ion concentration. Therefore, the final ER value of the low mix ratio case in Fig. 12 was slightly lower than that of the high mix ratio case in Fig. 9. The difference in the flow velocity of grout fluid could be another factor affecting the final reduced value of the electrical resistivity. However, to verify this relationship, we need a quantitative study in which we monitor, in real-time, the ER according to different flow velocities under various w/c mix ratio conditions.

For the case of aperture size 5 mm with w/c 0.6, Fig. 13 shows visual images of the grout penetration behavior and the change of electrical resistivity with elapsed time. The time to completely fill the fracture cell with aperture size 5 mm at w/c of 0.6 was about 180 s. Compared to the case of the same aperture size at w/c 1.0, the penetration speed of the injected grout decreased by 1.2 times because the viscosity increased 15 times (from 22 to 327 cP). Compared to the case of different aperture size (10 mm) at the same w/c ratio (0.6), the penetration speed of the injected grout decreased by 2.4 times because the aperture size was doubled (from 5 to 10 mm). This result indicates that the influence of the aperture size on the speed of grout penetration can be greater than that of the viscosity change due to the w/c ratio. Like as in all other cases, the change of electrical resistivity from 73 to 2 Ω·m showed a clear trend

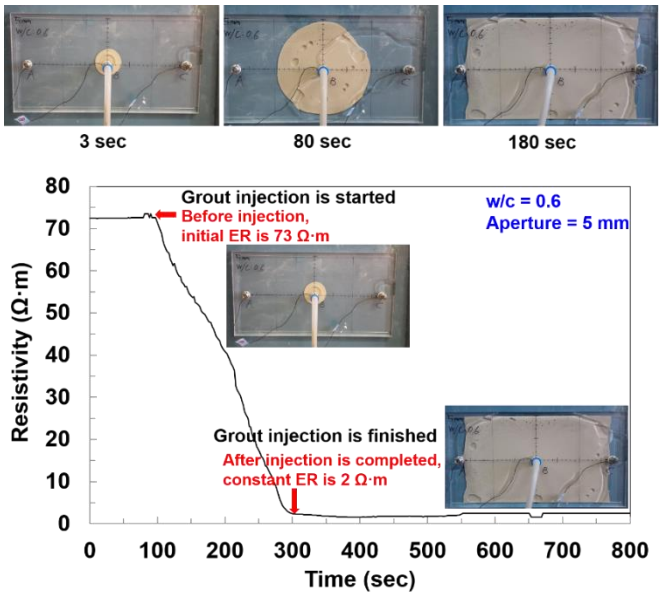

Fig. 13 Grout penetration images and electrical resistivity results with elapsed time for w/c = 0.6 and aperture size = 5 mm

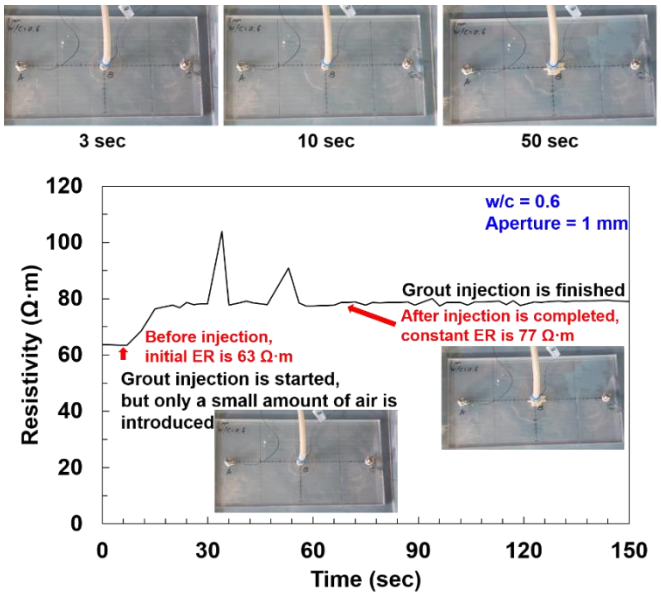

Fig. 14 Grout penetration images and electrical resistivity results with elapsed time for w/c = 0.6 and aperture size = 1 mm

of reduction despite the presence of small air bubbles.

Fig. 14 shows visual images of the grout penetration behavior and change of the electrical resistivity with elapsed time for the case of aperture 1 mm with w/c = 0.6. Early in the sequence (at time 10 s), a number of small air bubbles were injected into the center port of the fracture cell for a while. However, the grout fluid did not penetrate the interior of the fracture under these conditions and the injection was stopped after 50 s. The small aperture size and low w/c ratio (i.e., high viscosity: 327 cP) made it difficult for the grout mixture to move, which caused failure of the grout injection and penetration in this case (aperture 1 mm, w/c 0.6).

In an additional experiment, injection was tried again at the side ports (A and C) with the flow rate increased to 3000 mL/min. Despite the high injection rate, grout penetration failed very early, and the final distribution of the injected grout was also limited to the vicinity of the side ports, as shown in Fig. 15.

Because proper injection and penetration of grout failed in this case, the change pattern of electrical resistivity was different from all other previous experimental cases. After starting grout injection, the electrical resistivity value increased slightly from 63 to 77 Ω·m. This is because only a small amount of air was introduced for the first 10 s. Then, the electrical resistivity was constant until the injection was completed, because there was no more grout injection and penetration into the acrylic fracture. Consequently, the electrical resistivity measurement well-reflected the process of incomplete injection, which offers an effective indicator for detecting the failure of a grouting operation.

In summary, a key point here is that change in the

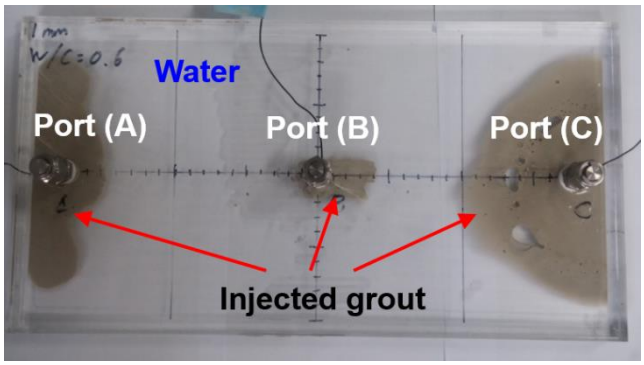

Fig. 15 Grout injection into ports A and C for w/c = 0.6 and aperture size = 1 mm

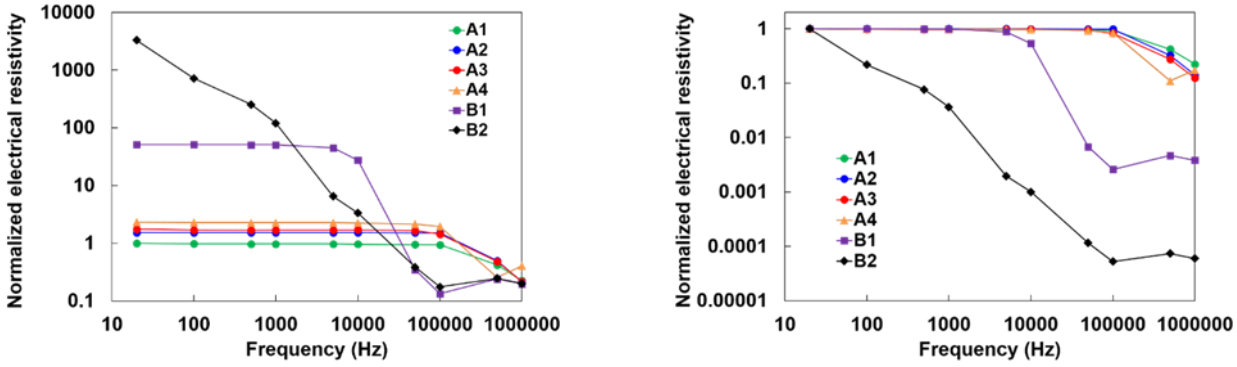

Fig. 16 Normalized electrical resistivity according to frequency variation after grout curing: (a) Result of normalizing based on the lowest value for which the largest flow channel exists (standard value: aperture 10 mm and w/c 1.0 at frequency of 20 Hz) and (b) Result of normalizing based on the value at the lowest frequency of 20 Hz for each experimental case

pattern (timing and degree) related to the electrical resistivity are the most important indicators of grout penetration, rather than the absolute value by itself. In other words, the point at which the resistivity begins to drop suddenly indicates the time at which the grout penetrates the fracture test cell, and decrease of the electrical resistivity by more than one order compared to the initial value, means that the grout fluid has completely penetrated and is distributed within the space between the measuring electrodes.

4.3 Electrical resistivity monitoring after grout curing

Once the grout fluid has penetrated into rock fractures near an underground structure, it hardens with elapsed time. During this hardening (curing) process, the grout material gains mechanical strength. Therefore, estimating the distribution and compactness of grouting after the curing process in the target area is directly related to evaluation of the grouting performance for such as waterproofing efficiency.

In this experiment, the electrical resistivity according to frequency (20 Hz to 1 MHz) was measured and analyzed for the test cells in which grout penetration and the curing process were completed. All electrical resistivity values were normalized and displayed for easy comparison of the grouting status. The status was divided into two groups: grouting with open flow channels (Group A) and grouting perfect for waterproofing (Group B). This classification was only about the grouting waterproofing efficiency after curing of the grout (see Table 1).

Fig. 16(a) shows the electrical resistivity normalized by the lowest value (obtained with aperture of 10 mm, w/c of 1.0, and frequency of 20 Hz). For Group A in Table 1, normalized electrical resistivity with a constant value of 1, was observed in the frequency range from 20 to 100 kHz. In these three cases (A1, A2, and A3), a continuous water flow channel (air space or void) was commonly observed at the upper part of the tested cell. This upper flow channel can be formed by the bleeding phenomenon, also called water separation from the grout mixture, which occurs during the hardening process (Lee *et al.* 2017). This incomplete sealing by grouting can lead to water leakage into the grouted underground structure over the long term.

For Case A4 (aperture 1 mm with w/c of 0.6), the normalized electrical resistivity was constant in the frequency range <100 kHz, which was similar to the previous three cases (A1, A2, and A3) where continuous flow paths existed. For A4, an isolated water storage area (water reservoir) was widely observed except around the inlet and outlet ports where the electrodes were installed. However, there were no connective flow passages due to the local sealing of grouting in the vicinity of the electrode ports (Fig. 15).

Table 1 Classification according to grouting condition after the curing process

Group		Experimental cases (aperture with w/c)	Normalized electrical resistivity at frequency of 20 Hz	Description
A	1	10 mm with 1.0	1.0 (standard value)	Grouting with open flow channel /Low waterproof efficiency
	2	5 mm with 1.0	1.5	Grouting with open flow channel /Low waterproof efficiency
	3	10 mm with 0.6	1.7	Grouting with open flow channel /Low waterproof efficiency
	4	1 mm with 0.6	2.3	Grouting with closed flow channel / Existence of isolated water reservoir
B	1	1 mm with 1.0	51	Perfect sealing / High compactness
	2	5 mm with 0.6	3,310	Perfect sealing / High compactness

For Group B (perfect sealing and high compactness), the normalized electrical resistivity had a relatively high and constant value of 51 at frequencies<5 kHz for B1; thereafter, the resistivity decreased with increasing frequency. For B1, the inside of the tested cell was perfectly sealed by hardened grouting without any voids. It was also observed for B2 that the fracture cell was completely sealed by cured grouting without any voids. B2 did not have a connected flow channel. The normalized electrical resistivity showed a very high value (3310) at the lowest frequency (20 Hz). This resistivity sharply decreased with increase in frequency.

In the two cases above (B1 and B2), although the observed grouting conditions were almost identical and with perfect sealing, there was a difference in the length of frequency section with a constant value and the initial value of the normalized electrical resistivity. This difference is due to the compactness of the cured grouting. The hardened grouting in the fracture with aperture of 5 mm and w/c 0.6 (B2) was more compact than that of the fracture with aperture of 1 mm and w/c 1.0 (B1). This is because a low w/c ratio means a greater amount of micro cement than water in the grout. Overall, it was confirmed that the frequency section having a constant value became shorter as the internal texture of the grouting became denser, and without any internal void space (constant section length: B2 < B1). In addition, the electrical resistivity values were clearly different according to the degree of compactness of the grouting. As shown in Table 1, the maximum normalized electrical resistivity value (3310) of high compactness was higher than that (51) of low compactness by approximately two orders of magnitude.

Fig. 16(b) shows the electrical resistivity normalized by the value at the lowest frequency (20 Hz) for each experimental case. As a whole, a constant value of normalized electrical resistivity was observed at frequency<100 kHz when water remained in the fracture cell after grout curing (A1, A2, A3, and A4). Moreover, the trend of decrease of the normalized electrical resistivity was > 100 kHz for Group A.

However, when the inside of a fracture cell was completely sealed and no water was present within voids (B1 and B2), the frequency range having a constant value was further shortened to 5 kHz or less. Moreover, as the internal texture of the grouting became denser and more tightly bonded between particles, the constant frequency range became shorter and the sensitivity of the resistivity reduction became much higher. The degree of maximum decrease of normalized electrical resistivity according to the frequency was 2.6E-03 and 5.3E-05 based on the initial value at 20 Hz in the case of B1 and B2, respectively. From this result, we can infer whether there is water remaining in the grouted zone and what the compactness of the filled grouting is by analyzing the change behaviors of the normalized electrical resistivity value according to the frequency alteration.

In summary, it is possible to estimate directly the grouting condition of the target area between the electrodes by estimating change of the normalized electrical resistivity according to the frequency. This can be applied to evaluation of the grouting performance such as for waterproofing efficiency. For reference, there is a slight difference in the resistivity value according to the size and degree of void space within which water exists within the fracture after grouting. However, this difference is relatively small compared to the cases of complete sealing due to grouting. This is because there is an obvious large difference in the maximum value and in the trend of change of normalized electrical resistivity between the case of void space existing within the grouting and the case of perfect sealing. In future study, it is necessary to generalize the correlation between the grouting state and the electrical resistivity by collecting change data from a greater variety of experimental cases.

5. Discussion: Field-monitoring scenario with electrical resistivity monitoring

After the precise comparison of electrical resistivity and visual observation of grout penetration/distribution in the laboratory experiments, an electrical resistivity monitoring system is proposed as a potential method for indirectly detecting grout penetration and for evaluating grouting performance (e.g., for waterproofing efficiency) in rock fractures. When the electrical resistivity monitoring system is applied in the field for such as in situ underground structures, it can be conceptually explained as follows.

First, Fig. 17(a) and 17(b) show the concept for detecting the penetration and distribution of grout fluid injected into boreholes. Multiple installations of two or more electrodes per borehole are recommended. When a current (voltage) is passed through a pair of electrodes

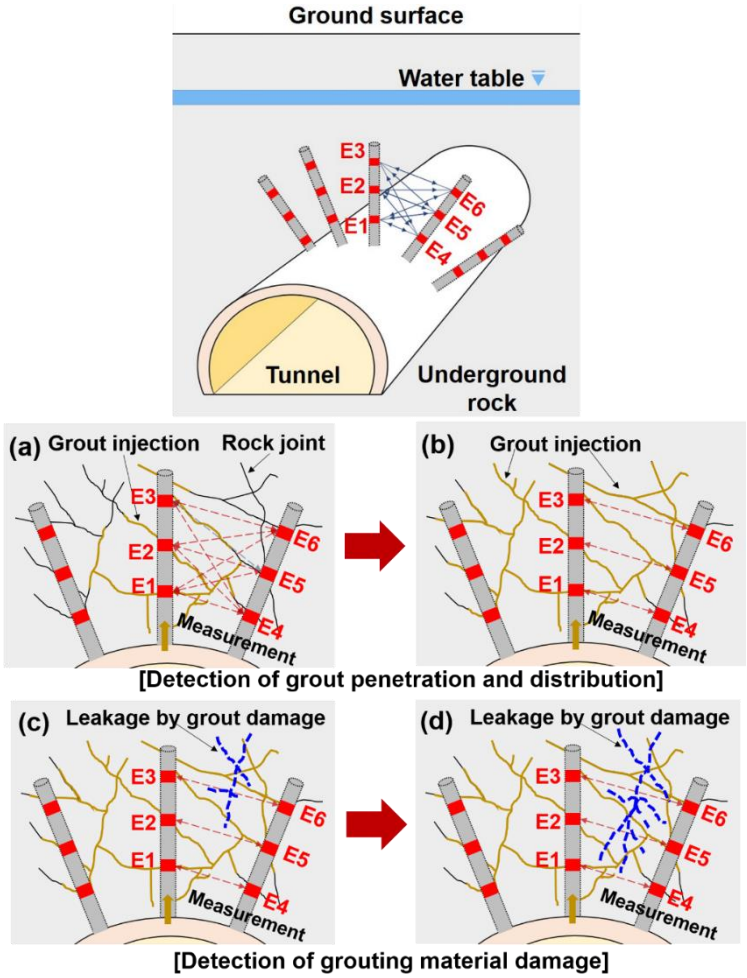

Fig. 17 Applicability of the electrical resistivity monitoring system

(a designated electrode and the other electrode), the resistivity value between the electrodes can be measured. If E4, E5, and E6 electrodes are used in pairs of electrodes based on the A1 reference electrode, it is possible to evaluate the grout penetration according to the injection depth. In addition, if E2 and E3 electrodes are used as a pair of electrodes based on the E1 reference electrode, it is possible to detect the grout penetration inside the borehole. For the sake of understanding, it can be confirmed that the grouting injection is completed in the target section when the electrical resistivity is measured using electrodes E1–E4 under the grouting injection condition in Fig. 17(a). On the other hand, when the electrical resistivity is measured using the E3-E6 electrodes, it can be judged whether the grouting is completed. In this way, the degree of grouting of the target area can be evaluated using the combinations of electrodes. If the grouting is distributed as shown in Fig. 17(b), it can be estimated that the grouting is properly completed through the electrical resistivity values in the E1–E4, E2–E5, and E3–E6 sections. Moreover, even if the grout has completely penetrated and become distributed, incomplete sealing may occur due to bleeding (water separation), which can also be detected through real-time monitoring based on electrical resistivity.

Second, Fig. 17(c) and 17(d) show examples of grouting damage due to weathering, earthquake, and deterioration. If the grouting in the rock is damaged, the stability of the underground structure may be lowered and groundwater may reach the inside of the underground structure. As shown in Fig. 17(c), when the groundwater penetrates due to grouting damage, the electrical resistivity will be changed in the E3-E6 section (or in the E3-E5 and E2-E6 sections). If a change in electrical resistivity value occurs in the E1-E4 section (Fig. 17(d)), it can be judged that groundwater infiltration has occurred around the underground structure. In other words, a warning system can be operated by sensing the change of electrical resistivity using a system of installed electrode sensors. Because the installed electrodes can be made permanent, the electrical resistivity system could provide a long-term method for safety monitoring of rock grouting.

6. Conclusions

After the work reported in this paper, we proposed an electrical resistivity monitoring system as a new method for detecting grout penetration and for evaluating the grouting performance within rock fractures. For this purpose, grout injection tests were performed using a transparent fracture

replica with apertures of various sizes and with varying water/concrete ratios. The feasibility of our non-destructive method was verified by comparing electrical resistivity with visual observations of grout penetration and distribution. In addition, the characteristics of normalized electrical resistivity were verified for cured grout in relation to an applied frequency.

• The injected grout showed a variety of penetration patterns according to the fracture size and w/c ratio, which matched well the pattern of change (timing and degree of decrease) of electrical resistivity, in real time, in all the experimental cases.

• As the grout penetrated, the electrical resistivity values decreased very rapidly to less than ~ 1 order of the initial values (before starting grout injection) in all cases. Then, after completion of the grout injection process, a final, much-decreased value of electrical resistivity due to grout penetration became constant.

• The electrical resistivity monitoring system well-detected abnormal situations such as the unexpected air injection and grouting injection failure.

• After the curing process, as the compactness of the grouting increased and the amount of void space decreased, the maximum value of the normalized electrical resistivity became larger and the frequency section length having a constant value became shorter.

• The proposed electrical resistivity method could be used for long-term monitoring of grouting performance and stability in underground rock structures in the field.

Acknowledgments

This work was supported by the National Research Foundation of Korea (NRF) grant funded by the Korea Government (MSIT) (No. NRF-2019R1G1A1100517) and the Basic Research and Development Project of the Korea Institute of Geoscience and Mineral Resources (KIGAM), which was funded by the Ministry of Science, ICT, Republic of Korea.

References

Axelsson, M., Gustafson, G. and Fransson, Å. (2009), "Stop mechanism for cementitious grouts at different water-to-cement ratios", *Tunn. Undergr. Sp. Tech.*, **24**(4), 390-397. https://doi.org/10.1016/j.tust.2008.11.001.

Broch, E. (2007), "Use of the underground in the city of Trondheim, Norway", *Proceedings of the 11th ACCUS Conference: Expanding the Frontiers*, Athens, Greece, September.

Chen, Y., Nishiyama, T., Terada, M. and Iwamoto, Y. (2000), "A fluorescent approach to the identification of grout injected into fissures and pore spaces", *Eng. Geol.*, **56**, 395-401. https://doi.org/10.1016/S0013-7952(99)00100-3.

Eriksson, M. (2002), "Grouting field experiment at the Äspö hard rock laboratory", *Tunn. Undergr. Sp. Tech.*, **17**(3), 287-293. https://doi.org/10.1016/S0886-7798(02)00024-X.

Funehag, J. and Fransson, Å. (2006), "Sealing narrow fractures with a Newtonian fluid: Model prediction for grouting verified by filed study", *Tunn. Undergr. Sp. Tech.*, **21**(5), 492-498. https://doi.org/10.1016/j.tust.2005.08.010.

Gueddouda, M.L., Lamara, M., Abou-bekr, N. and Taibi, S. (2010), "Hydraulic behaviour of dune sand bentonite mixtures under confining stress", *Geomech. Eng.*, **2**(3), 213-227. https://doi.org/10.12989/gae.2010.2.3.213.

Gustafson, G. and Stille, H. (1996), "Prediction of groutability from grout properties and hydrogeological data", *Tunn. Undergr. Sp. Tech.*, **11**(3), 325-332. https://doi.org/10.1016/0886-7798(96)00027-2.

Henderson, A.E., Robertson, I.A., Whitfield, J.M., Garrard, G.F.G., Swannell, N.G. and Fisch, H. (2008), "A new method for real-time monitoring of grout spread through fractured rocks", *MRS Proc.*, **1107**. https://doi.org/10.1557/PROC-1107-577.

Høien, A.H. and Nilsen, B. (2014), "Rock mass grouting in the Løren tunnel: Case study with the main focus on the groutability and feasibility of drill parameter interpretation", *Rock Mech. Rock Eng.*, **47**(3), 967-983. https://doi.org/10.1007/s00603-013-0386-7.

ISRM. (1978), "Suggested methods for the quantitative description of discontinuities in rock masses", *Int. J. Rock Mech. Min. Sci. Geomech.*, **15**(6), 319-368. https://doi.org/10.1016/0148-9062(78)91472-9.

Keller G.V. and Frischknecht F.C. (1996), *Electrical Methods in Geophysical Prospecting*, Pergamon Press Inc., Oxford, U.K.

Khave, G.J. (2014), "Delineating subterranean water conduits using hydraulic testing and machine performance parameters in TBM tunnel post-grouting", *Int. J. Rock Mech. Min. Sci.*, **70**, 308-317. https://doi.org/10.1016/j.ijrmms.2014.04.013.

Kim, H.M., Lee, J.W., Yazdani, M., Tohidi, E., Nejati, H.R. and Park, E.S. (2018), "Coupled viscous fluid flow and joint deformation analysis for grout injection in a rock joint", *Rock Mech. Rock Eng.*, **51**(2), 627-638. https://doi.org/10.1007/s00603-017-1339-3.

Kobayashi, S., Soyq, M., Takeuchi, J., Nobuto, A., Nakaya, A., Okuno, T., Shimada, S., Kaneto, T. and Majima, T. (2014), "Rock grouting and durability experiments of colloidal silica at Kurashiki underground LPG storage base", *Proceedings of the ISRM Regional Symposium - EUROCK 2014*, Vigo, Spain, May.

Lee, H., Oh, T.M., Park, E.S., Lee, J.W. and Kim, H.M. (2017), "Factors affecting waterproof efficiency of grouting in single rock fracture", *Geomech. Eng.*, **12**(5), 771-783. https://doi.org/10.12989/gae.2017.12.5.771.

Lisa, H., Christina, B., Åsa, F., Gunnar, G. and Johan, F. (2012), "A hard rock tunnel case study: Characterization of the water-bearing fracture system for tunnel grouting", *Tunn. Undergr. Sp. Tech.*, **30**, 132-144. https://doi.org/10.1016/j.tust.2012.02.014.

Lunn, R.J., Corson, L.T., Howell, C., El Mountassir, G., Reid, C. and Harley, S.L. (2018), "Could magnetic properties be used to image a grouted rock volume?", *J. Appl. Geophys.*, **155**, 162-175. https://doi.org/10.1016/j.jappgeo.2018.06.015.

Madhavi, T.Ch. and Annamalai, S. (2016), "Electrical conductivity of concrete", *ARPN. J. Eng. Appl. Sci.*, **11**(9), 5979-5982.

Majer, E. L. (1989), "The application of high frequency seismic monitoring methods for the mapping of grout injections", *Int. J. Rock Mech. Min. Sci. Geomech. Abstr.*, **26**(3-4), 249-256. https://doi.org/10.1016/0148-9062(89)91974-8.

Mohajerani, S., Baghbanan, A., Bagherpour, R. and Hashemolhosseini, H. (2015), "Grout penetration in fractured rock mass using a new developed explicit algorithm", *Int. J. Rock Mech. Min. Sci.*, **80**, 412-417. https://doi.org/10.1016/j.ijrmms.2015.06.013.

Mohammed, M.H., Pusch, R. and Knutsson, S. (2015), "Study of cement-grout penetration into fractures under static and oscillatory conditions", *Tunn. Undergr. Sp. Tech.*, **45**, 10-19. https://doi.org/10.1016/j.tust.2014.08.003.

Northcroft, I.W. (2006), "Innovative materials and methods for

ground support, consolidation and water sealing for the mining industry", *J. S. Afr. I. Min. Metall.*, **106**(12), 835-844.
Oh, T.M., Cho, G.C. and Lee, C.H. (2014), "Effect of soil mineralogy and pore water chemistry on the electrical resistivity of saturated soils", *J. Geotech. Geoenviron. Eng.*, **140**(11), 06014012. https://doi.org/10.1061/(ASCE)GT.1943-5606.0001175.
Panthi, K.K. and Nilsen, B. (2010), "Uncertainty for assessing leakage through water tunnels: A case from Nepal Himalaya", *Rock Mech. Rock Eng.*, **43**(5), 629-639. https://doi.org/10.1007/s00603-009-0075-8.
Rafi, J.Y. and Stille, H. (2014), "Control of rock jacking considering spread of grout and grouting pressure", *Tunn. Undergr. Sp. Tech.*, **40**, 1-15. https://doi.org/10.1016/j.tust.2013.09.005.
Saeidi, O., Stille, H. and Torabi, S.R. (2013), "Numerical and analytical analyses of the effects of different joint and grout properties on the rock mass groutability", *Tunn. Undergr. Sp. Tech.*, **38**, 11-25. https://doi.org/10.1016/j.tust.2013.05.005.
SsangYong Cement Inc. (2016), http://www.ssangyongcement.co.kr/jsp.
Stille, H., Gustafson, G. and Hassler, L. (2012), "Application of new theories and technology for grouting of Dams and foundations on rock", *Geotech. Geol. Eng.*, **30**(3), 603-624. https://doi.org/10.1007/s10706-012-9512-7.
Wang, J.B., Liu, W.R., Huang, Y.X. and Zhang, X.C. (2015), "Prediction model of surface subsidence for salt rock storage based on logistic function", *Geomech. Eng.*, **9**(1), 25-37. https://doi.org/10.12989/gae.2015.9.1.025.
Zhang, D., Fang, Q. and Lou, H. (2014), "Grouting techniques for the unfavorable geological conditions of Xiang'an subsea tunnel in China", *J. Rock Mech. Geotech. Eng.*, **6**(5), 438-446. https://doi.org/10.1016/j.jrmge.2014.07.005.
Zhang, F., Xie, X. and Huang, H. (2010), "Application of ground penetrating radar in grouting evaluation for shield tunnel construction", *Tunn. Undergr. Sp. Tech.*, **25**(2), 99-107. https://doi.org/10.1016/j.tust.2009.09.006.
Zhang, Q., Xu, Z., Wu, J. and He, P. (2017), "Grouting effects evaluation of water-rich faults and its engineering application in Qingdao Jiaozhou Bay Subsea Tunnel, China", *Geomech. Eng.*, **12**(1), 35-52. https://doi.org/10.12989/gae.2017.12.1.035.

IC